2018 IEEE-RAS 18th International Conference on Humanoid Robots (Humanoids)
Beijing, China, November 6-9, 2018

Passivity-Based Compliant Walking on Torque-Controlled Hydraulic Biped Robot

Kenta Hirayama, Nozomu Hirosawa, and Sang-Ho Hyon

***Abstract*— This paper presents an experimental evaluation of passivity-based whole-body motion control framework for compliant walking. The controller computes joint torques without requiring much computation cost and contact force measuring. Instead of limiting the walking speed slow (static walking), in this work we specifically address the difficulties of walking on unstable and uneven ground. No terrain information is used in the experiments, that is, the ground is assumed to be flat, and the desired motion trajectories are given offline. With this setup we evaluate the terrain adaptability by force control alone. The controller is applied to our torque-controllable hydraulic humanoid robot, TaeMu. The robot could walk on a rocker board stably, and even climbed the small step with a little modification of the controller (quasi-dynamic walking).**

I. Introduction

A. Background

Humans can walk stably on various ground conditions without precise information related to its roughness, stiffness, or friction. One reason is that each joint moves flexibly that the legs adapt to external forces and the environment.

Some works have examined such human-like walk in biped robots. The most basic method is (position-based) impedance control [1] [2], where the desired position is modified according to the desired impedance model and the measured force from the sensors. Using this method, robots respond to external forces only at the place where the force sensor is attached, and only to the direction of the sensing axis. This makes the compliance and adaptability quite limited.

Therefore, some researchers have been trying to achieve them with direct joint torque control. One of the authors (Hyon) in ATR proposed a passivity-based whole-body motion control framework for humanoid robots with redundant joints and multiple contact points [3]. Then, they demonstrated dynamic balance control [4] using the SARCOS hydraulic humanoid robots [5]. They also applied the controller to three-dimensional dynamic walking in simulation [3]. Nevertheless, they were unable to make it come to real because of the lack of capabilities of actuators. Ott et al. [6] in DLR invented a passivity-based method combined with contact wrench optimization using a quadratic programming (QP), and realized compliant balancing on their biped robot.

Recently, many researchers have proposed rich model-based compensation and optimization methods [7] [8] [9]. For these methods, both the complete set of dynamics and precise state estimation are necessary. The high computation cost and tuning methods of many design parameters in the optimization are subjects to be resolved for implementation. Regardless of the methods, however, it is still unclear what the minimum set of control and estimation necessary to achieve tasks on given humanoid robot hardware are.

This work was supported by the Futaba Research Grant Program of the Futaba Foundation.

All the authors are with Humanoid Systems Laboratory, Ritsumeikan University (Noji-Higashi 1-1-1, Kusatsu, Shiga 525-8577, Japan). sangho@ieee.org

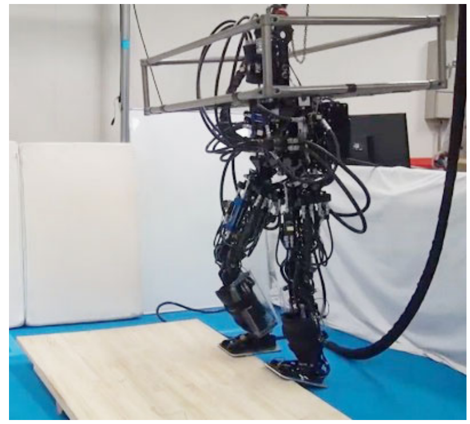

Fig. 1. Torque-controlled hydraulic humanoid robot TaeMu climbing up a rocker board. The robot has the height of 1.41 m and the weight of 62.25 kg. The rocker board has the length of 1.2 m and the width of 0.9 m. The height of the rocking axis is 0.07 m, and the maximum slope is 5 deg. The upper body joints are disabled in this work.

B. Contribution

Based on the background and motivation, we have been trying to develop our own hardware (of unlimited use) in Ritsumeikan University to evaluate the true performance of the existing methods including ours. Recently we have finished prototyping the robot TaeMu (Fig. 1). This torque-controlled life-size hydraulic humanoid robot has 3-DoF in its body and 12-DoF on its legs. It has the height of 1.41 m and the weight of 62.25 kg in this study (when the weight is removed from the upper body). Joints are actuated by hydraulic cylinders and linkage mechanisms. Joint torques are computed using measured forces of each cylinder and moment arms computed from joint angles. In addition, the CoM position is estimated by joint angles and body posture measured by the IMU. The detailed mechanical design, joint specifications, and the experimental results on *dynamic* double-support balancing are presented in [10].

From engineering point of view, it is important to clarify systematically the guaranteed performance of the employed algorithms within tolerance of accuracy of model, etc. Therefore, we use simple solutions to address real problems and

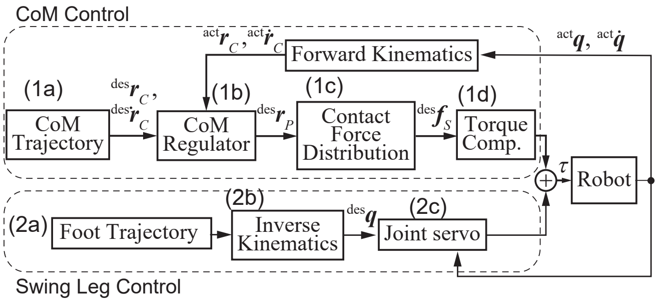

Fig. 2. Control architecture of biped walking. It consists of the CoM controller and the swing leg controller. The outputs of the controllers are summed up and commanded to the robot.

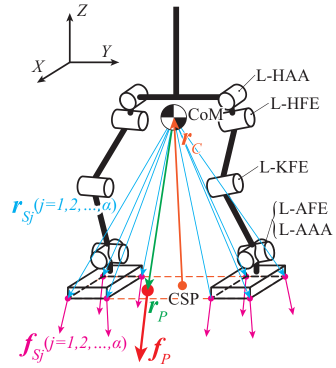

Fig. 3. Definition of coordinates, joint names, and position/force vectors that used in the controller. The upper body joints are disabled.

gradually update the solution as needed. As a good starting point, we chose the passivity-based solutions because we know *it works*. Then we will try to find what else is really necessary to enhance the performance.

Since we have already succeeded in compliant balancing [10], we address the compliant biped walking in this paper. To clarify the performance step by step, we limit the scope to *static* walking. This does not mean the passivity-based approach cannot be applied to *dynamic* walking. Actually, in our simulation study [10] a biped robot walked stably even under strong external perturbations. Passivity-based approach is aimed at simple, yet practical method to cope with *dynamic* motion control, as the readers can capture the underlying principle from many literatures [11], [12].

Instead of limiting the walking speed slow, in this work we specifically address the difficulties of walking on unstable and uneven ground. The desired center of mass (CoM) trajectory and the swing leg trajectory are given in advance. The CoM is controlled by a combination of optimal contact force control and a simple CoM regulator based on a point-mass model.

We evaluated biped walking control experiments on level ground and on unstable ground for evaluation of compliant force control. The ground is assumed to be flat, and no terrain information is used in these experiments. With this setup we can evaluate the terrain adaptability by *force control alone*.

The construction of this paper is the following. First, we show the control framework and review the passivity-based force control in Section II. Next, we show experimental results of biped walking with the TaeMu robot in Section III and discuss the performance. Finally, we conclude this report in Section IV.

II. Control Framework

A. Overview

The overall control architecture for biped walking is shown in Fig. 2. It consists of the CoM controller and the Swing leg controller. The CoM controller has three parts: (1a) CoM trajectory generator, (1b) CoM regulator, (1c) Contact force distribution, and (1d) Joint torque computation.

The CoM regulator (1b) assumes so-called CoM-ZMP model to compute the desired center of pressure (CoP) on the ground so that the CoM tracks the desired trajectories. It consists of feed-forward term and state feedback term (PD control) with gravity compensation. Although there are numerous ways to determine the PID gains, we tuned the gains by hand.

The contact force distributer (1c) employs the optimal contact force controller [4], then, they are converted to whole-body joint torque in (1d). In (1a), the desired CoM trajectory with constant height is generated by a smooth cubic function of time, which connects positions of the two supporting feet. The robot coordinate system is at center of support polygons (CSP), hence the coordinate system is changed when each supporting foot switches.

The swing leg controller has two parts: (2a) Trajectory generator, (2b) Inverse kinematics, and (2c) Joint servo controller. The swing leg trajectory is also a cubic function of time, which starts from the position of supporting foot at the moment of the lift-off. In (2c) the PD gains are set constant. However, the gains for the ankle joint are lowered before touchdown so that the foot naturally adapts to the ground.

With this simple method, designable parameters that should be tuned are only CoM and base orientation feedback gains and position feedback gains for swing leg. The commanded joint torques are sent to the low-level servo-controllers (not shown in this diagram), where high-speed torque feedback controller with the measured joint torques (via load cells attached to hydraulic cylinders) is implemented.

B. Optimal contact force control

This section presents the core of the optimal contact force control [4] combined with QP solver as presented in [6]. The controller is implemented in (1c), (1d) in Fig. 2.

Fig. 3 shows the coordinates and related variables of the biped model. $\boldsymbol{r}_C = [x_C, y_C, z_C]^{\mathrm{T}} \in \mathbb{R}^3$ is the CoM position in a coordinate system based on the CSP. $\boldsymbol{r}_P = [x_P, y_P, z_P]^{\mathrm{T}} \in \mathbb{R}^3$ represents the position vector of CoP measured from the CoM, and $\boldsymbol{f}_P = [f_{xP}, f_{yP}, f_{zP}]^{\mathrm{T}} \in \mathbb{R}^3$ stands for the ground applied force (GAF) on CoP. The GAF is equal to the sum of the contact forces. $\boldsymbol{r}_s = [\boldsymbol{r}_{S1}^{\mathrm{T}}, \boldsymbol{r}_{S2}^{\mathrm{T}}, \cdots, \boldsymbol{r}_{S\alpha}^{\mathrm{T}}]^{\mathrm{T}} \in \mathbb{R}^{3\times\alpha}$ is the position vector of α contact points measured from CoM.

$\boldsymbol{f}_s = [\boldsymbol{f}_{S1}^{\mathrm{T}}, \boldsymbol{f}_{S2}^{\mathrm{T}}, \cdots, \boldsymbol{f}_{S\alpha}^{\mathrm{T}}]^{\mathrm{T}} \in \mathbb{R}^{3\times\alpha}$ is the associated contact force on the contact points. Each element is a 3D vector, that is, $\boldsymbol{r}_{Sj} = [x_{Sj}, y_{Sj}, z_{Sj}]^{\mathrm{T}} \in \mathbb{R}^3$, $\boldsymbol{f}_{Sj} = [f_{xSj}, f_{ySj}, f_{zSj}]^{\mathrm{T}} \in \mathbb{R}^3$.

From the relations between GAF and CoP:

$$\boldsymbol{f}_P = \sum_{j=1}^{\alpha} \boldsymbol{f}_{Sj}, \tag{1}$$

$$x_P = \frac{\sum_{j=1}^{\alpha} x_{Sj} f_{zSj}}{\sum_{j=1}^{\alpha} f_{zSj}}, \quad y_P = \frac{\sum_{j=1}^{\alpha} y_{Sj} f_{zSj}}{\sum_{j=1}^{\alpha} f_{zSj}}, \tag{2}$$

the equation related to the vertical contact force $\boldsymbol{f}_{zS}$ can be written as:

$$\underbrace{\begin{bmatrix} x_P \\ y_P \\ 1 \end{bmatrix}}_{\boldsymbol{b}_z \in \mathbb{R}^3} f_{zP} = \underbrace{\begin{bmatrix} x_{S1} & x_{S2} & \cdots & x_{S\alpha} \\ y_{S1} & y_{S2} & \cdots & y_{S\alpha} \\ 1 & 1 & \cdots & 1 \end{bmatrix}}_{\boldsymbol{A}_z \in \mathbb{R}^{3\times\alpha}} \underbrace{\begin{bmatrix} f_{zS1} \\ f_{zS2} \\ \vdots \\ f_{zS\alpha} \end{bmatrix}}_{\boldsymbol{f}_{zS} \in \mathbb{R}^{\alpha}}. \tag{3}$$

Similarly, equations related to horizontal contact forces $\boldsymbol{f}_{xS}$ and $\boldsymbol{f}_{yS}$ can be written as:

$$\underbrace{\begin{bmatrix} y_P \\ z_P \\ 1 \end{bmatrix}}_{\boldsymbol{b}_x \in \mathbb{R}^3} f_{xP} = \underbrace{\begin{bmatrix} y_{S1} & y_{S2} & \cdots & y_{S\alpha} \\ z_{S1} & z_{S2} & \cdots & z_{S\alpha} \\ 1 & 1 & \cdots & 1 \end{bmatrix}}_{\boldsymbol{A}_x \in \mathbb{R}^{3\times\alpha}} \underbrace{\begin{bmatrix} f_{xS1} \\ f_{xS2} \\ \vdots \\ f_{xS\alpha} \end{bmatrix}}_{\boldsymbol{f}_{xS} \in \mathbb{R}^{\alpha}}, \tag{4}$$

$$\underbrace{\begin{bmatrix} x_P \\ z_P \\ 1 \end{bmatrix}}_{\boldsymbol{b}_y \in \mathbb{R}^3} f_{yP} = \underbrace{\begin{bmatrix} x_{S1} & x_{S2} & \cdots & x_{S\alpha} \\ z_{S1} & z_{S2} & \cdots & z_{S\alpha} \\ 1 & 1 & \cdots & 1 \end{bmatrix}}_{\boldsymbol{A}_y \in \mathbb{R}^{3\times\alpha}} \underbrace{\begin{bmatrix} f_{yS1} \\ f_{yS2} \\ \vdots \\ f_{yS\alpha} \end{bmatrix}}_{\boldsymbol{f}_{yS} \in \mathbb{R}^{\alpha}}. \tag{5}$$

Solving underdetermined equations (3), (4) and (5) for $\boldsymbol{f}_{zS}$, $\boldsymbol{f}_{xS}$ and $\boldsymbol{f}_{yS}$, one obtains the desired distributed force $\overline{\boldsymbol{f}}_s$ at each contact point. In this study, we computed unilateral solution $\overline{\boldsymbol{f}}_s > 0$ through a QP solver. Note that (4) and (5) are different from what we have been using in [3].

Finally, in passivity-based approach, the $\overline{\boldsymbol{f}}_s$ is transformed to desired joint torques with the contact Jacobian matrix $\boldsymbol{J}_s = \frac{\partial \boldsymbol{r}_s}{\partial \boldsymbol{q}}$ and joint damping coefficient $\boldsymbol{D} > 0$.

$$\overline{\boldsymbol{\tau}} = \boldsymbol{J}_s^{\mathrm{T}} \overline{\boldsymbol{f}}_s - \boldsymbol{D}\dot{\boldsymbol{q}}, \tag{6}$$

where $\boldsymbol{q} \in \mathbb{R}^n$ is the active joint coordinate. In addition, we compute the stabilizing moments for the base orientation (roll and pitch) and superpose them to the hip joints. Note that the stabilizing moments for the base orientation (including the yaw axis) can be put into the optimization process as presented in [3].

III. Experiment

We experimented *blind* static walking on stable level ground and unstable uneven ground. A priori environment recognition and terrain information input are not used in the experiments. Walking parameters, for example, footstep and walking cycle are set offline on the assumption that the ground is even. The footstep is 0.2 m in X-axis direction, 0.3 m in Y-axis direction, the foot lifting height is 0.2 m, the period of CoM transfer is 2.0 s, and the period of swing leg is 1.5 s; the walking cycle is 3.5 s. The foot has the length of 0.25 m and the width of 0.15 m. In this work, we disabled 3-DoF in the body and two pelvis joints, and used only 10-Dof of legs.

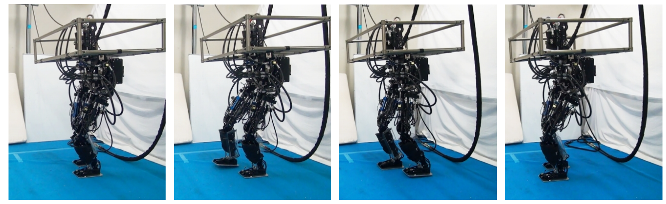

Fig. 4. Picture sequence (from left to right) showing the TaeMu robot walking on level ground. The interval between each picture is 2 s.

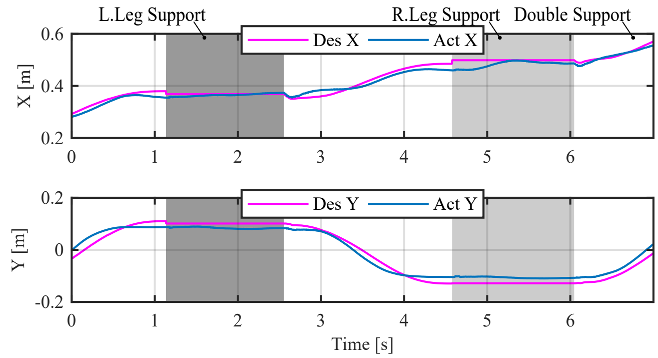

Fig. 5. Time history of estimated CoM position of static walking on level ground.

A. Blind static walk on level ground

Fig. 4 shows the picture sequence of the robot walking on level ground (see also the attached video). Fig. 5 shows the CoM position roughly tracks the desired trajectories. The light gray regions indicate the right leg support, and the dark gray regions indicate the left leg support, and the white regions indicate both legs support. The desired CoM trajectory is changed to the constant value in single leg

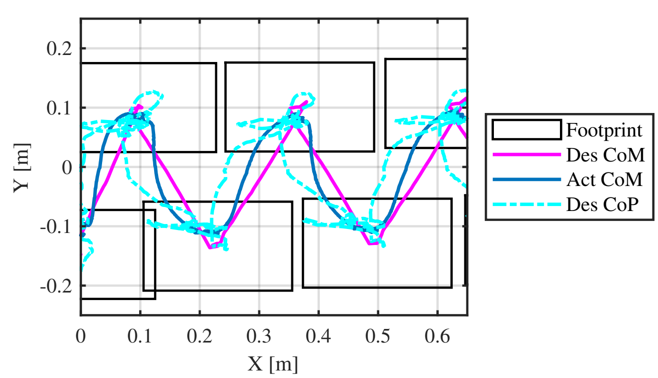

Fig. 6. Position of the estimated CoM, desired CoP and footprint of the static walking (from left to right) on level ground.

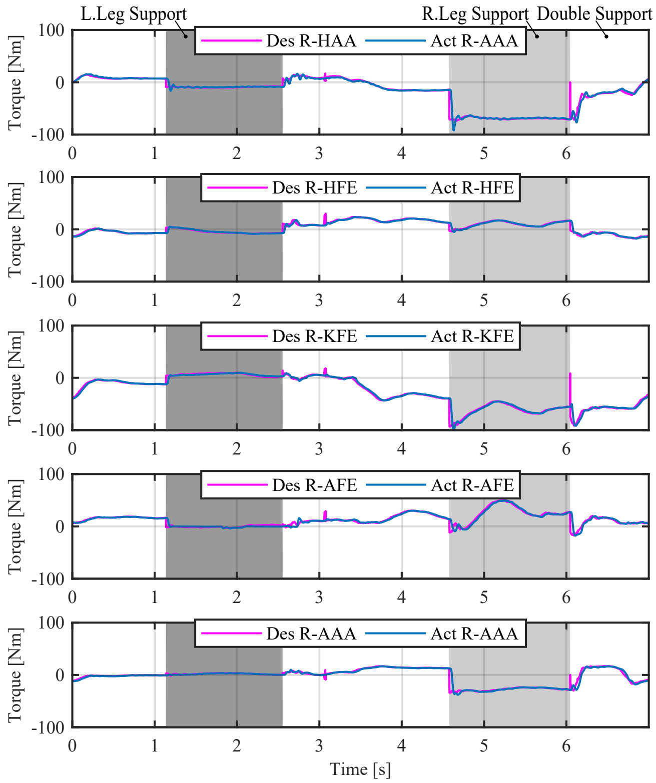

Fig. 7. Joint torques which of the right leg during the static walking.

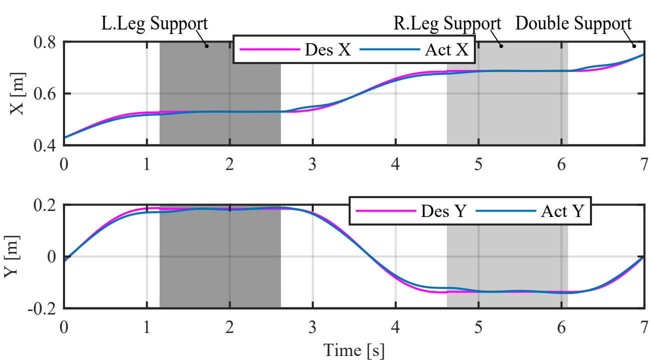

Fig. 8. [Simulation] Time history of CoM position of static walking on level ground.

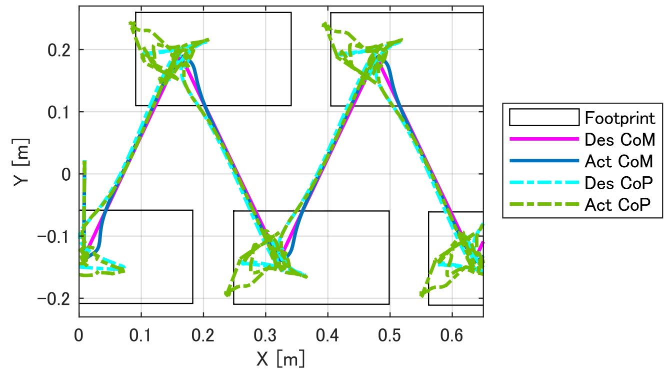

Fig. 9. [Simulation] Position of CoM, desired CoP, actual CoP and footprint of static walking (from left to right) on level ground.

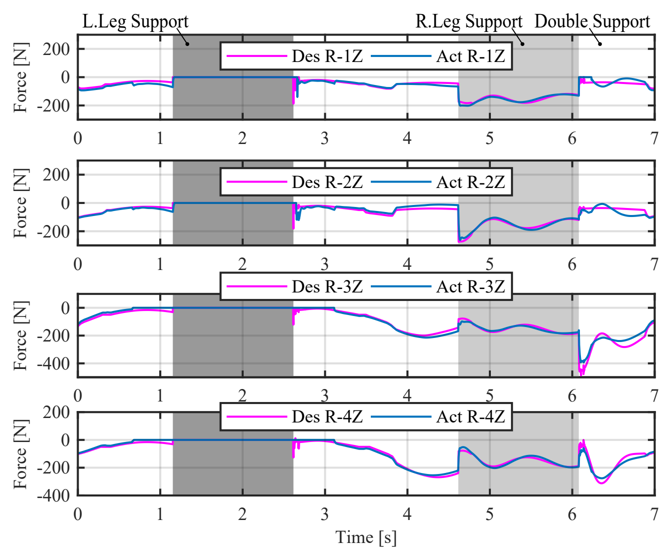

Fig. 10. [Simulation] Time history of Z-axis contact forces at the four vertices of the right foot.

support when the CoM sufficiently reached the stable region of the desired supporting polygon. Therefore, some jumps are caused in the desired trajectory. The steady-state error is 3 cm, which is within the foot area.

The relations among the CoM, the CoP and supporting foot areas during a walk are shown in Fig. 6. One can observe significant tracking errors in the CoM trajectory. The reason is that we could not increase the PD gains to avoid vibration that comes from the natural frequency of the mechanical flexibility as well as the hydraulic compressibility.

On the other hand, the actual joint torques thoroughly track the desired trajectories as can be seen from Fig. 7. Joint torque controllability is the key points in our control framework. In our robot, we employ an active force feedback where the force is measured from the load cell attached to the cylinder. Some literatures on a hydraulic humanoid robot (ATLAS) describe that the robot is implemented with a hybrid position and torque control law, where the force is measured via pressure sensors on each chamber of the cylinders [7] [13]. It is noteworthy, however, that the performance of the torque control is not clear as the controller is used for joint motion trajectory control [7], where the desired joint acceleration is integrated to the velocity, and utilized as feedforward term (to the servo valve current) in addition to the torque control to obtain better motion trajectory tracking.

Control performance of joint torque directly affect to that of contact forces. Unfortunately, in our case, the contact forces are not measured because the TaeMu robot has no force sensors on its sole (ongoing work). However, we can expect contact forces track the desired trajectories. This can be validated through the simulation as follows.

Fig. 8 shows the CoM tracking of the simulated biped under exactly the same condition as the experiment. The relations among the CoM, the CoP and supporting foot areas during a walk are shown in Fig. 9. The simulated contact forces (simple spring-damper model) on four contact

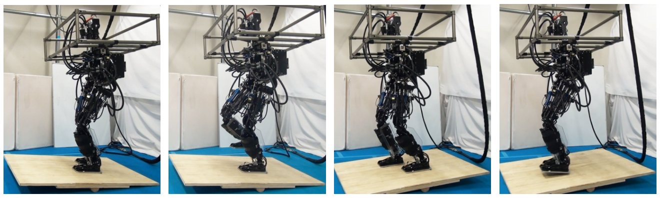

Fig. 11. Picture sequence (from left to right) showing the TaeMu robot walking on a rocker board at right angles to the rocking axis. The interval between each picture is 2 s. The rocker board has the length of 1.2 m, the width of 0.9 m, the maximum height of 0.07 m at the rocking axis, and the maximum slope of 5 deg.

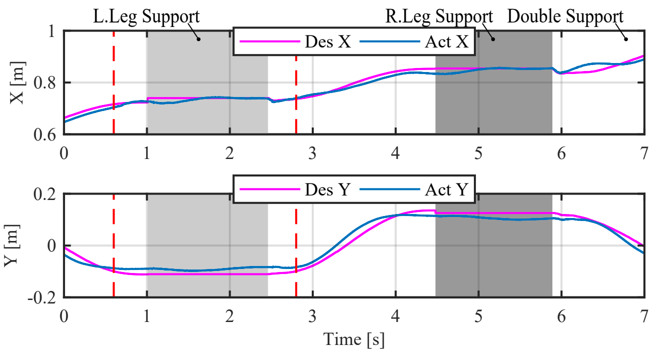

Fig. 12. Time history of the estimated CoM position of the same experiment (Fig. 11). The rocker board rocked the slope two times between the red dashed lines.

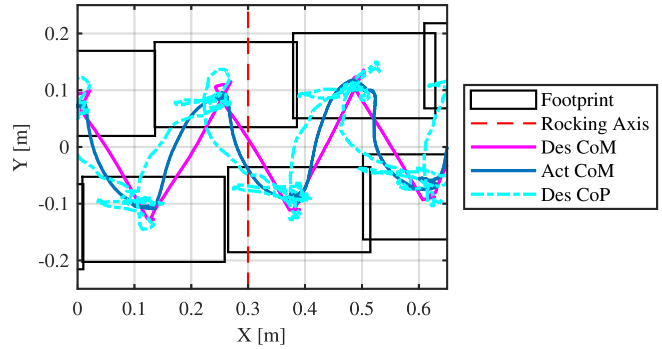

Fig. 13. Position of the estimated CoM, desired CoP and footprint of the same experiment (Fig. 11). The robot walks from left to right.

points on the right foot are shown in Fig. 10. These two graphs shows the simulated contact forces track the desired trajectories thoroughly as long as the commanded whole-body joint torques are exactly generated at the joints.

On the other hand, some spikes can be observed in the "desired" joint torque both in the experiment and simulation. We found these spikes come from the unexpected errors in the controller implementation. The possible reason is that QP solver did not converge within the control cycle (2ms) especially when there are instantaneous changes of the contact point allocation. We are investigating the problem [1]. Note that the actual joint torque cannot follow the spikes anyway. Therefore, this error does not affect the validity of the method.

B. Blind static walk on unstable ground

We also experimented with walking on an unstable rocker board. The rocker board has the length of 1.2 m, the width of 0.9 m, and the maximum height of 0.07 m at the rocking axis, and the maximum slope of 5 deg.

Fig. 11 shows the picture sequence of the robot walks at *right angles* to rocking axis (see also the attached video). In spite of the sudden changing of the slope, the robot walked without falling down. Although the walking parameters were set in advance on the assumption that the ground is even, the force controller made the foot to fit the slope and kept balance against the shaking. The trajectory tracking of CoM position is shown in Fig. 15, and the light gray regions indicate the right leg support, and the dark gray regions indicate the left leg support, and the white regions indicate both legs support. The rocker board rocked its slope two times between the red dashed lines.

The relations among the CoM, the CoP and supporting foot areas can be seen from Fig. 13, where the red dashed line shows the approximate position of the rocking axis. In this experiment, footprints are laterally drifting. The drift comes from the unanticipated slope and the CoM tracking error. Also, the desired CoM trajectory is given in the CSP coordinate; hence the robot does not know how much the robot moved in the world coordinate frame. This problem can be solved easily, and is not the subject of this paper.

C. Blind quasi-dynamic walk on unstable ground

Finally, we will show the results of the robot walking on the same rocker board, but in *parallel* to rocking axis. Fig. 14 shows the picture sequence of the robot walking (see also the attached video). The robot not only could walk on the laterally rocking board, but also could climb it up and down.

However, with the static walking pattern used in Section III-B, the robot failed to climb the board due to the large reaction force. Therefore, we modified the desired CoM position to the center of the next supporting foot when the actual CoM exits from the other foot. The walking parameters were also modified. Specifically, we set the footstep for X-axis and Y-axis to 0.2 m and 0.25 m, respectively, and time duration for DS and SS to 1.5 s and 1.2 s, respectively. As a result, the CoM is not always above the supporting area as can be seen from Fig. 15. This means the walking gait is *quasi-dynamic*.

The relations among the CoM, the CoP and supporting foot areas can be seen from Fig. 16. The light pink region shows the approximate position of the rocker board and the red dashed line shows the approximate position of the rocking axis. Fig. 17 highlights the instances of the climbing up and down the board.

IV. Conclusion

The passivity-based contact force control was evaluated through the experiments of blind static walking with the

[1]The updated experimental results will soon be presented in our website. http://www.humanoidsystems.org/blog/research_e

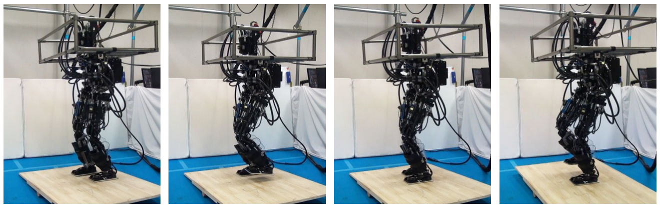

Fig. 14. Picture sequence (from left to right) showing the TaeMu robot walking on a rocker board in parallel to the rocking axis.

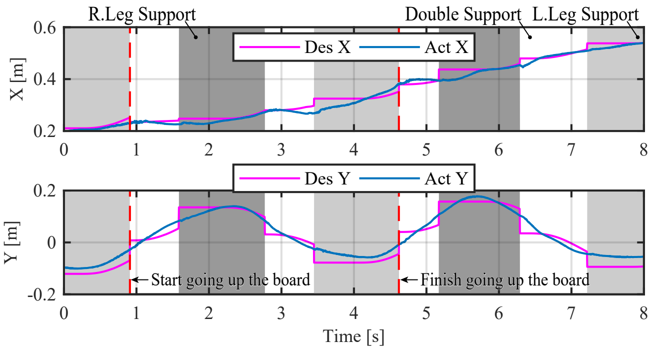

Fig. 15. Time history of the CoM position in the same experiment (Fig. 14).

biped robot TaeMu. The robot could walk on a rocker board stably, and even climbed the small step with a little modification of the controller (quasi-dynamic walking). We provided the technical details and real data of experiments.

The experimental data shown in this paper and the robot demonstration in the attached video, together with our previous experimental results [10], prove the effectiveness of our torque-controlled robot and the simple control architecture. There are no special tricks to conceal.

Although recently we witness great success of Boston Dynamics Inc. in their sophisticated hydraulic humanoid robot ATLAS that can perform dynamic walking, running, and even flipping [14], this paper shows the first successful experimental result of passivity-based biped walking on a torque-controlled hydraulic robot, which is not made by the same company.

As ongoing works, we try to quantitatively analyze the degree to which the tracking performance and terrain adaptation depend on the torque controllability or servo actuator characteristics. Robust and fast 3D dynamic walking will be the next target. We will enjoy a *long way* [15] to the goal.

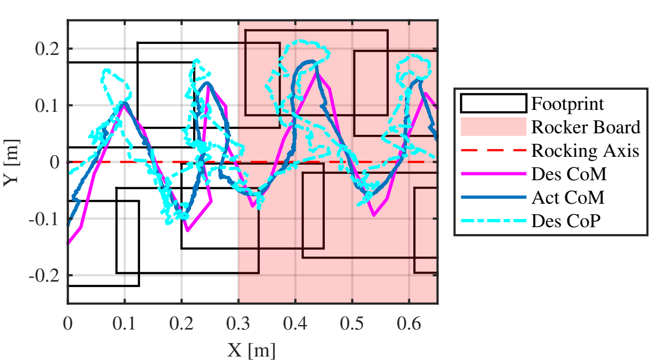

Fig. 16. Position of the estimated CoM, desired CoP and footprint of the same experiment (Fig. 14). The robot walks from left to right.

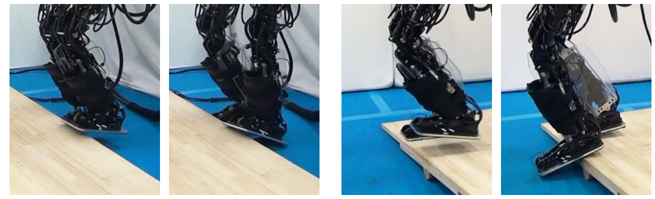

Fig. 17. Picture sequence showing foot adaptation when walking up (left two) and walking down (right two).

REFERENCES

[1] K. Hirai, M. Hirose, Y. Haikawa, and T. Takenaka, "The development of Honda humanoid robot," in *IEEE International Conference on Robotics and Automation (ICRA)*, 1998, pp. 1321–1326.

[2] S. Lohmeier, T. Buschmann, and H. Ulbrich, "System design and control of anthropomorphic walking Robot LOLA," *IEEE/ASME Transactions on Mechatronics*, vol. 14, no. 6, pp. 658–666, 2009.

[3] S. Hyon and G. Cheng, "Passivity-based full-body force control for humanoids and application to dynamic balancing and locomotion," in *IEEE/RSJ International Conference on Intelligent Robots and Systems (IROS)*, 2006, pp. 4915–4922.

[4] S. Hyon, J.G. Hale and G. Cheng, "Full-body compliant human-humanoid interaction: Balancing in the presence of unknown external forces," *IEEE Transactions on Robotics*, vol.23, no.5, pp. 884–898, 2007.

[5] G. Cheng, S. Hyon, J. Morimoto, A. Ude, G. Colvin, W. Scroggin, and S. C. Jacobsen, "CB: A humanoid research platform for exploring NeuroScience," in *IEEE-RAS International Conference on Humanoid Robots (Humanoids)*, 2006, pp. 182–187.

[6] C. Ott, M. A. Roa, and G. Hirzinger, "Posture and Balance Control for Biped Robots based on Contact Force Optimization," in *IEEE-RAS International Conference on Humanoid Robots (Humanoids)*, 2011, pp. 26–33.

[7] S. Feng, E. Whitman, X. Xinjilefu, and C. G. Atkeson, "Optimization based full body control for the atlas robot," in *IEEE-RAS International Conference on Humanoid Robots (Humanoids)*, 2015, pp. 120–127.

[8] B. Henze, M. A. Roa, and C. Ott, "Passivity-based whole-body balancing for torque-conrolled humanoid robots in multi-contact scenarios," *The International Journal of Robotics Research*, vol. 35, no. 12, pp. 1–22, 2016.

[9] G. Wiedebach, S. Bertrand, T. Wu, L. Fiorio, S. McCrory, R. Griffin, F. Nori, and J. Pratt, "Walking on Partial Footholds Including Line Contacts with the Humanoid Robot Atlas," in *IEEE-RAS International Conference on Humanoid Robots (Humanoids)*, 2016, pp. 1312–1319.

[10] S. Hyon, D. Suewaka, Y. Torii, and N. Oku, "Design and Experimental Evaluation of a Fast Torque-Controlled Hydraulic Humanoid Robot," *IEEE/ASME Transactions on Mechatronics*, pp. 623–634, 2017.

[11] A. J. van der Schaft, *L2-Gain and Passivity Techniques in Nonlinear Control*, Springer, 1999.

[12] S. Arimoto, M. Sekimoto, H. Hashiguchi, and R. Ozawa, "Natural resolution of ill-posedness of inverse kinematics for redundant robots: a challenge to bernstein's degrees-of-freedom problem," *Advanced Robotics*, vol. 19, no. 4, pp. 401–434, 2005.

[13] M. Johnson, B. Shrewsbury, S. Bertrand, T. Wu, D. Duran, M. Floyd, P. Abeles, D. Stephen, N. Mertins, A. Lesman, J. Carff, W. Rifenburgh, P. Kaveti, W. Straatman, J. Smith, and G, "Team IHMC's Lessons Learned from the DARPA Robotics Challenge Trials," *Journal of Field Robotics*, vol. 32, no. 2, pp. 192–208, 2015.

[14] Boston Dynamics Inc. website [Online] Available: `https://www.bostondynamics.com/atlas`

[15] J. Englsberger, G. Mesesan, A. Werner, and C. Ott, "Torque-Based Dynamic Walking - A Long Way from Simulation to Experiment," in 2018 IEEE International Conference on Robotics and Automation (ICRA), 2018, pp. 440-447.